

Incremental Forming Simulation of Dimples for Solar Mirror Supports using Isogeometric Analysis

Wade Evans¹, Johannes Pottas¹, Lukas Leidinger², Amit Nair², Fabian Knieps³, Benjamin Liebscher³, John Holmes⁴, Joe Coventry⁴

¹Timestep Pty Ltd.

²ANSYS

³thyssenkrupp Rasselstein GmbH

⁴The Australian National University

1 Introduction

Heliostats are concentrating mirrors which track the sun to direct light onto a receiver in concentrating solar power (CSP) systems. Heliostat cost and performance are major contributors to the capital cost of CSP systems and their levelised cost of energy. For this reason, several existing heliostat mirror facet designs utilise low-cost stamped supports which are laminated to glass mirrors to impart stiffness and maintain shape accuracy of the optical surface, whether curved or flat.



Fig. 1: The Crescent Dunes tower CSP plant with 1.2 million m² aperture area [1, 2].

A novel mirror panel support with dimple-like protrusions (Figure 2), which is suitable for high-volume and low-cost production of high-precision mirror panels, has been developed at the Australian National University. Single-point incremental forming (SPIF) is used for prototyping of mirror supports and an adapted version of the process is being investigated for medium-volume production for pilot-scale CSP plants. Among other parameters, the design envelope for incrementally formed parts is partly constrained by the maximum achievable wall angle without material rupture. Isogeometric analysis (IGA) is evaluated in this study as a means of simulating the SPIF process to predict strain, thinning and displacement during SPIF which are important for estimating the likelihood of rupture. IGA and conventional finite element analysis (FEA) are compared to determine the relative modelling effort and computational cost, and simulation results from both approaches are compared with experimental results to assess the accuracy of the simulation methods.



Fig.2: A field trial of the new dimple mirror panel at a test site of the Commonwealth Scientific Industrial Research Organisation in Australia.

2 Incremental sheet forming

Several variants of incremental sheet forming exist, including SPIF and two-point incremental forming (TPIF). The subject of this study is the SPIF method in which a single smooth hemispherical tool moves along a computer numerically controlled (CNC) toolpath to incrementally deform a steel sheet into a three-dimensional (3D) shape. In most variations of SPIF, the blank is clamped along its edges to constrain it during forming. In some hybrid methods, a partial die may be placed under the sheet to improve the final shape accuracy of the formed component by supporting the regions of the component which will remain in the original plane of the blank.

The advantages of SPIF over conventional forming are the use of low-cost generic tooling and the ability to exploit greater formability in some materials. It is well-understood that materials will strain significantly more before fracture during incremental forming than during conventional stamping. An interesting theory, called the noodle theory, proposes that a specific type of material localisation plays an important role in SPIF [3]. In the SPIF process, the incremental approach is believed to introduce multiple new localisations in series. The cumulative strains over macroscopic length scales from these localisations might exceed the maximum strain achievable at a single localisation, as is typically observed in stamping.

2.1 Approximation of thinning in SPIF

In contrast to stamping, where material flows significantly in the planar direction of the blank, material movement in SPIF is primarily in the direction normal to the blank. As a result, strains are small in the direction parallel to the toolpath and large perpendicular to the toolpath. Since the volume of material is constant, the wall thickness of the formed component can be estimated with reasonable accuracy using

$$t_f = t_i \sin \theta$$

where t_i is the initial blank thickness, θ is the wall angle and t_f is the final blank thickness [4] as shown in Figure 3.

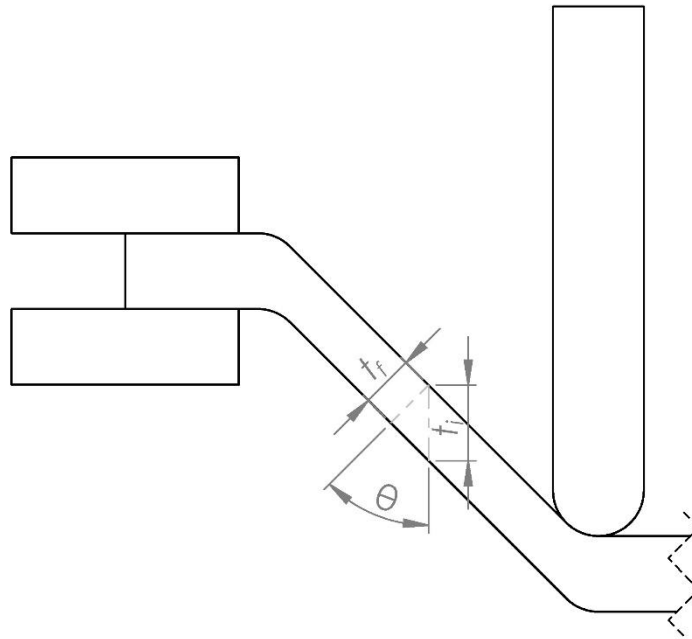


Fig.3: Diagram of a generic SPIF process showing the approximate relationship between initial and final thicknesses.

3 Isogeometric analysis

Isogeometric Analysis (IGA) was introduced in 2005 by Hughes et al. [5] with the goal to bring Computer Aided Design (CAD) and Finite Element Analysis (FEA) closer together by eliminating the burdensome meshing effort. To achieve this, the CAD geometry description based on Non-Uniform Rational B-Splines (NURBS) was also used for the analysis model, thus the term "isogeometric" analysis. The NURBS basis functions of higher order (degree) and higher continuity (max. inter-element continuity) fulfil all the analysis requirements such as partition of unity or linear independence and are therefore also used to describe the solution field (isoparametric concept). As a result, isogeometric analysis can be directly performed on accurate CAD geometries, instead of approximated, faceted FEA geometries (please note: as for FEA models, certain quality criteria should also be met for IGA models). Roughly speaking, IGA can be seen as FEA on CAD geometries, or FEA with spline basis functions.

Besides the advantages of a close connection between CAD and analysis, and an accurate IGA model geometry, it turned out that the NURBS basis functions also offer superior analysis properties compared to conventional Lagrange polynomials due to their higher inter-element continuity. This higher continuity may yield more accurate results due to a smooth solution field [6] and allows for a larger stable time step size in explicit dynamics [7].

Within LS-DYNA, isogeometric shell analysis is most advanced with several studies and successful applications in the field of explicit dynamic crash [8] and forming analysis [9, 10]. Such applications require capabilities like handling of nonlinear material behaviour, large deformations, contact, connections, boundary conditions, time step estimates or mass scaling, which are already available for IGA. For forming analysis, Hartmann et al. [9] and Hollweck et al. [10] report computationally more efficient simulations with IGA compared to conventional FEA for a comparable accuracy. Put differently, for a comparable simulation time, more accurate results are achieved with IGA. This is mainly because IGA permits a larger element size and a larger stable time step in explicit dynamics (for the same element size). Besides shells, also isogeometric solids are available and progressing rapidly [11].

Aims of this study are to evaluate the current IGA capabilities in LS-DYNA in the field of SPIF, to identify potential benefits, and to initiate further developments and improvements.

4 Experiments

4.1 Blank material

Investigations were conducted using TS275 material in 0.44 mm thickness, which was produced by thyssenkrupp Rasselstein. This ferritic low alloyed steel is typically used for applications in the metal packaging industry while showing a yield strength of about 275 MPa. To receive a precise description

of the plastic forming behaviour, different kinds of characterisation experiments were conducted. At the one hand tensile tests with a measuring length of 50 mm and optical measurement by using digital image correlation (DIC) were used to receive r-values and yield strength in three orientations ($0^\circ, 45^\circ, 90^\circ$) to the rolling direction. As well, the tensile test results were considered to describe the hardening behaviour in form of a flow curve. On the other hand, to expand the hardening description to higher strain values, bulge tests were conducted by using non-newton fluid. The bulge tests were also used to describe the biaxial strength behaviour which is essential when using yield locus models like Yld2000-2d. In the following the extrapolated flow curve as well as the yield locus described by the Yld2000-2d model can be observed.

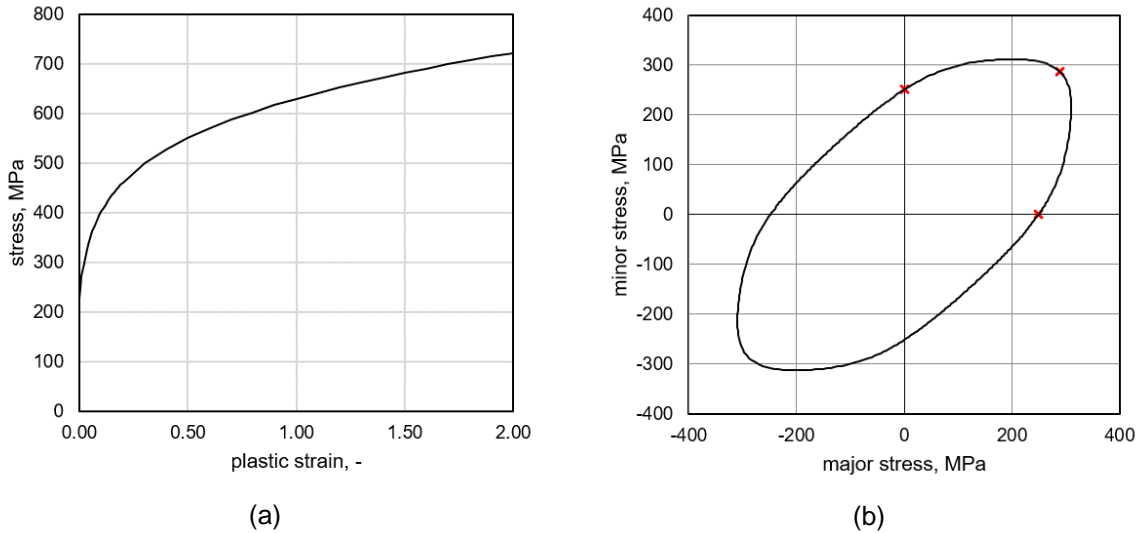


Fig.4: The (a) extrapolated flow curve and (b) yield locus model Yld200-2d for TS275 material.

4.2 Specimen geometry and toolpath

The specimen geometry was designed such that the wall angle, and therefore the likelihood of rupture, increases with forming depth. The region of interest of the specimen (the sidewall) was formed by rotating a circular arc about an axis to form a partial torus. A cross-section of the geometry of the specimen is shown Figure 5.

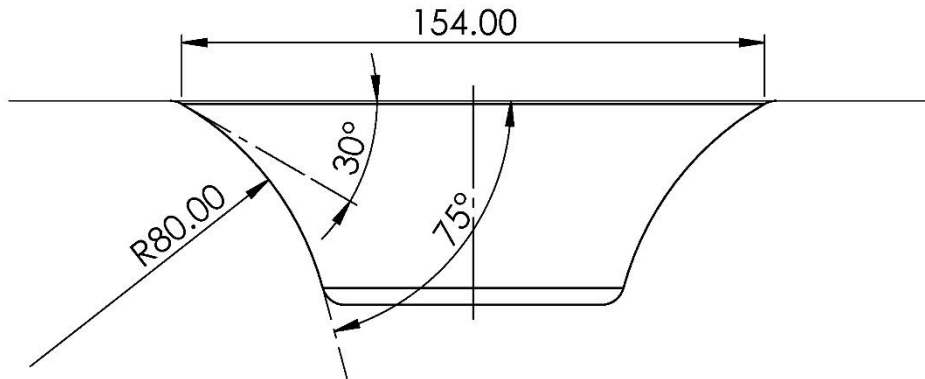


Fig.5: A cross-section of the SPIF test specimen geometry.

The toolpath was generated as a spiral pocketing operation using CAMWorks with 1.5 mm Z-step height.

4.3 Experimental setup

The experiment was conducted using a CNC router. A stand with clamping plates was mounted on the table of the machine. Each of the two clamping plates was a 245 x 245 mm steel plate with a 160 mm hole in the centre. The specimen was clamped between the two plates with sufficient force to prevent slipping during forming. A light coating of Coolube 2210 cutting lubricant was wiped onto the specimen with a clean cloth. A hemispherical forming tool with 12 mm diameter was zeroed on the top surface of the specimen at the centre of the clamping plate hole. The DIC strain measurement was initiated (refer to Section 4.4 for details) and the tool motion started. The tool was stopped after the specimen fractured. Figure 6 is an image series showing the progression of the forming process.

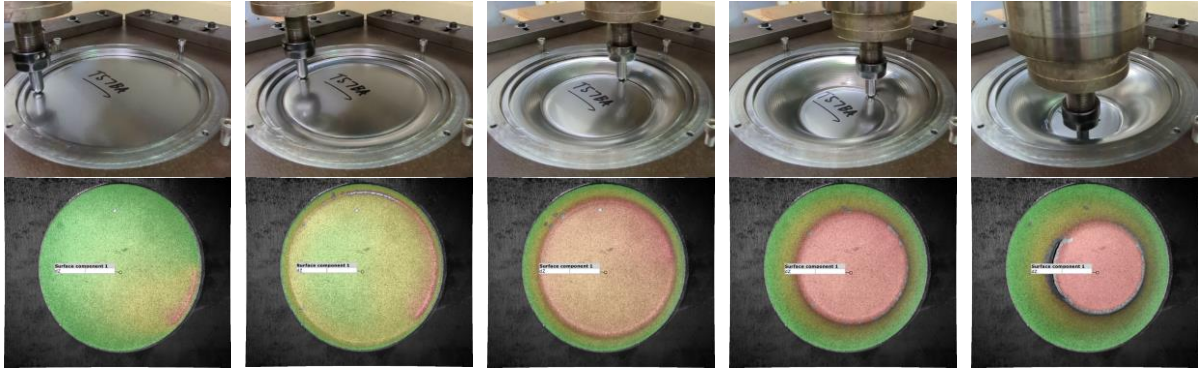


Fig.6: Image series showing the progression of the forming process to failure as viewed from above and from below with unscaled colour map of Z-displacements.

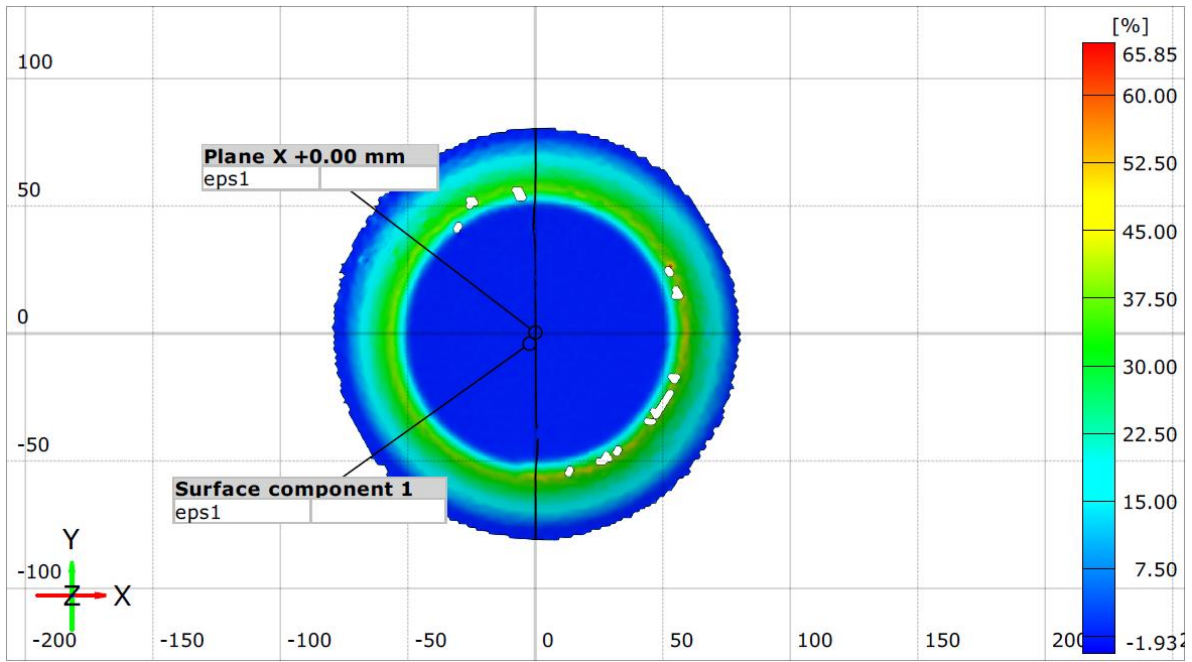
4.4 Strain measurement

Strain measurements were conducted using a Digital Image Correlation (DIC) system, ARAMIS version 6.3. Two cameras were positioned under the specimen to capture the 3D deformation and surface strain field as the specimen was deformed. Prior to testing, each specimen was sprayed with two layers of white undercoat and then with a black stochastic speckle pattern to enable tracking of surface points. The measuring volume was 180 mm by 215 mm with a depth of field of 50 mm. The camera's sensors had a resolution of 2448 by 2048 which resulted in an imaging resolution of around 11.4 pixels/mm. Due to the high strain localisation near the forming tip a balance between spatial resolution and accuracy was considered when selecting the subset size of 19 by 19 pixels (1.67 mm) and subset step of 16 pixels (1.41 mm). Using a series of images before forming, the random error in the measurements could be quantified, as described in previous research [12]. The in-plane displacement accuracy was found to be 0.003 mm and the out-of-plane 0.01 mm. Normal and principal strain accuracy was similarly quantified as 0.08% and thickness reduction as 0.11%.

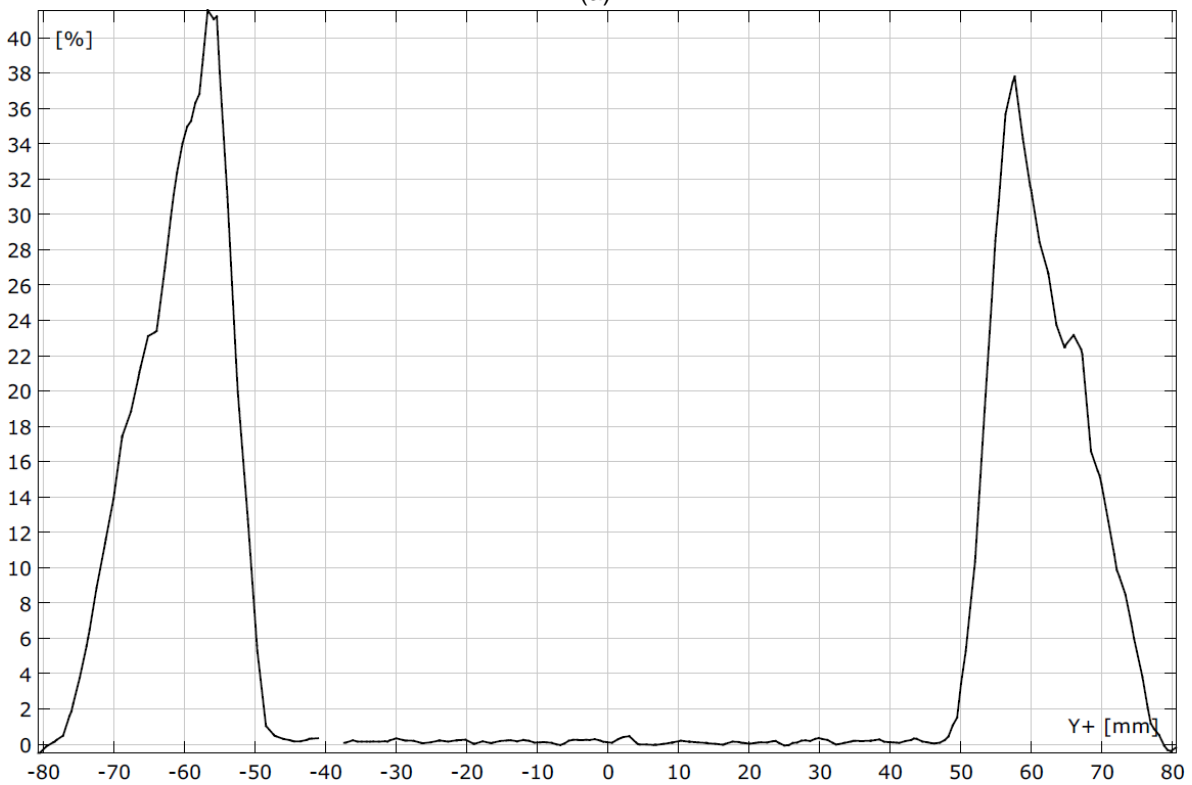


Fig.7: DIC strain measurement setup.

4.5 Experimental results

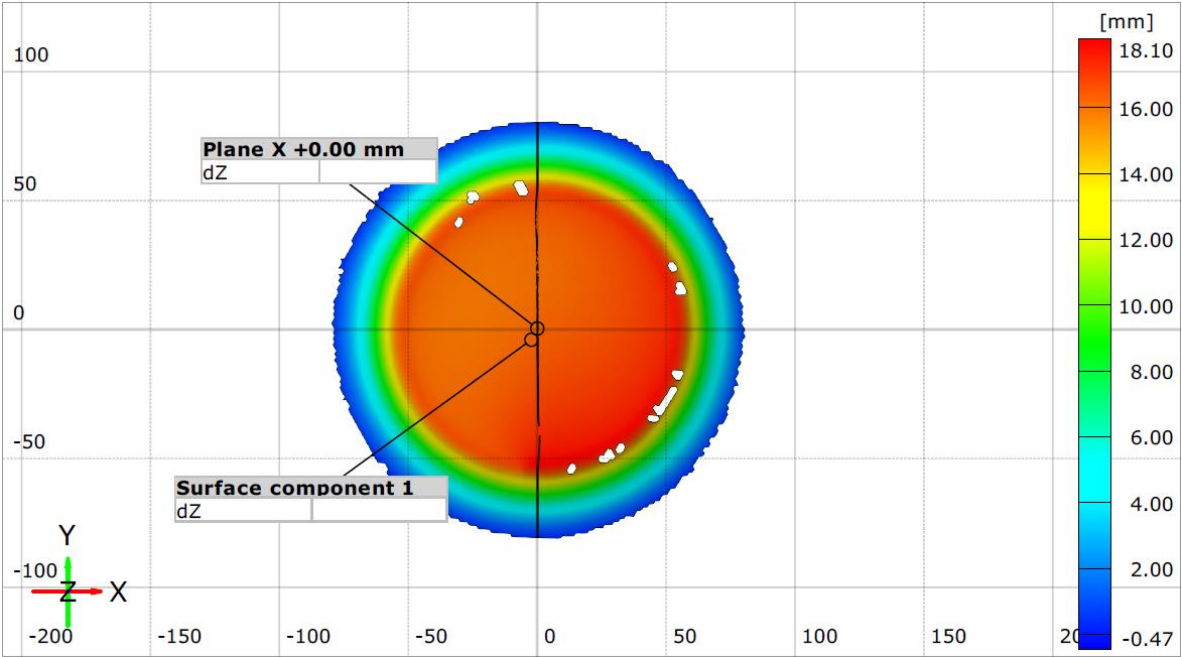


(a)

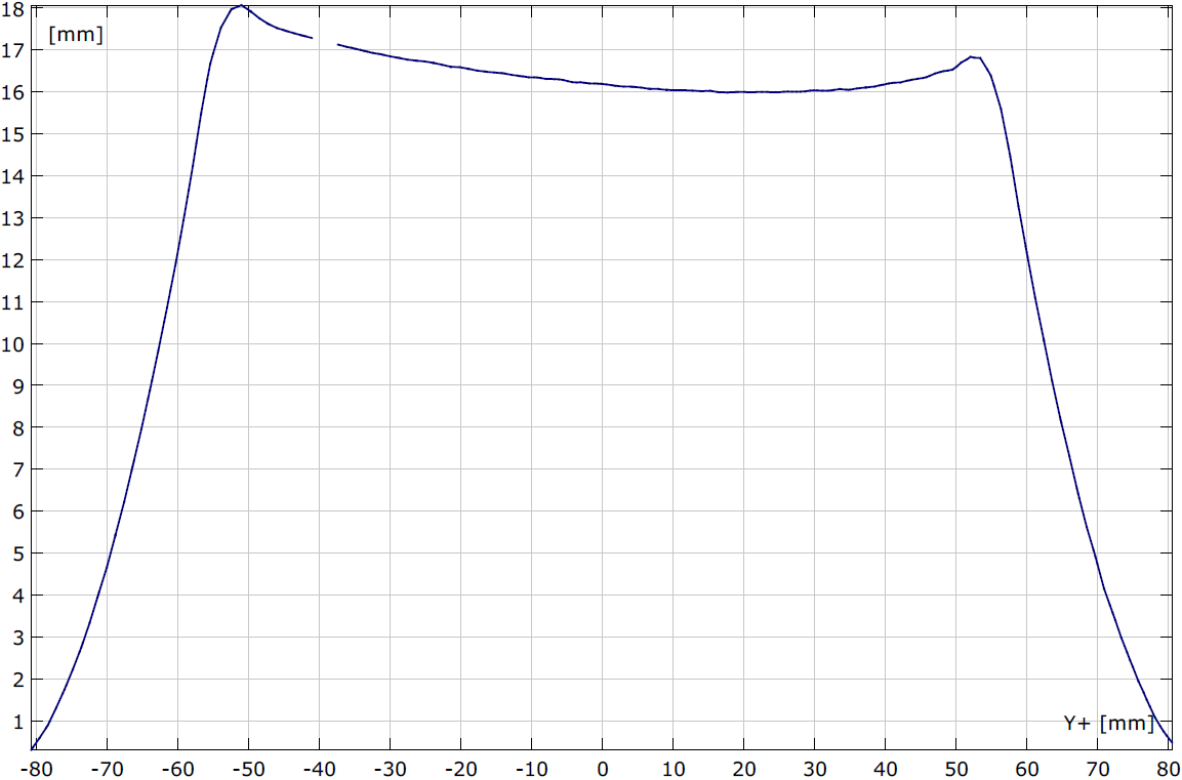


(b)

Fig.8: Maximum principal strains measured on the lower surface of the specimen at 98 s: (a) map, and (b) values along the intersection with the YZ-plane.

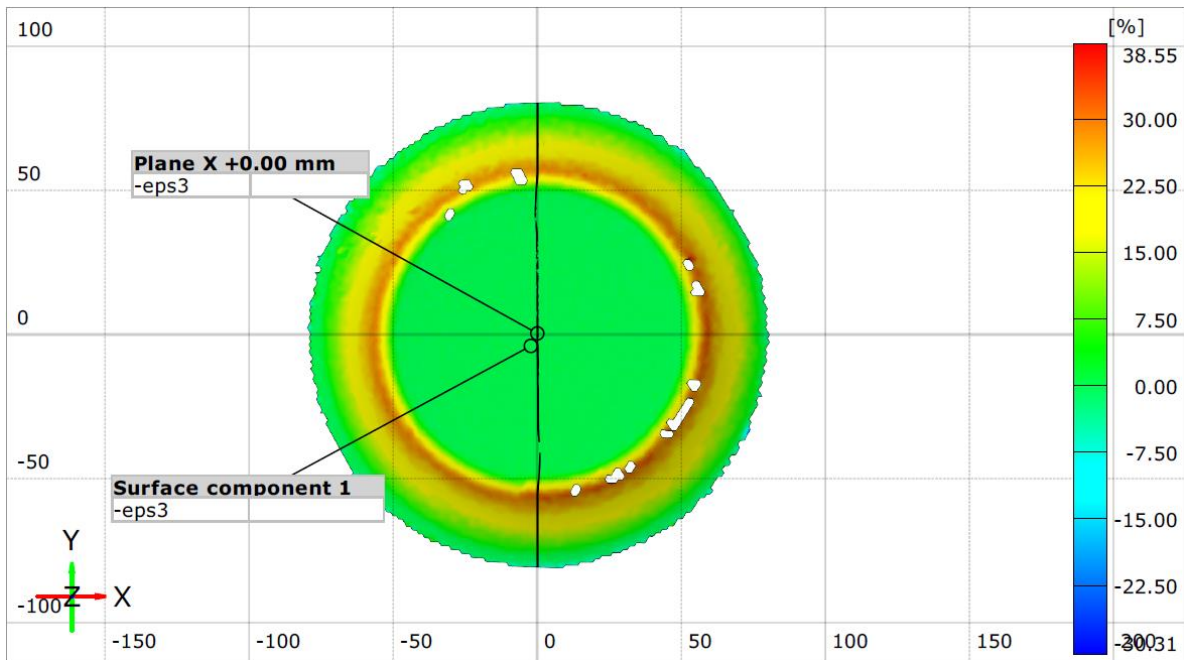


(a)

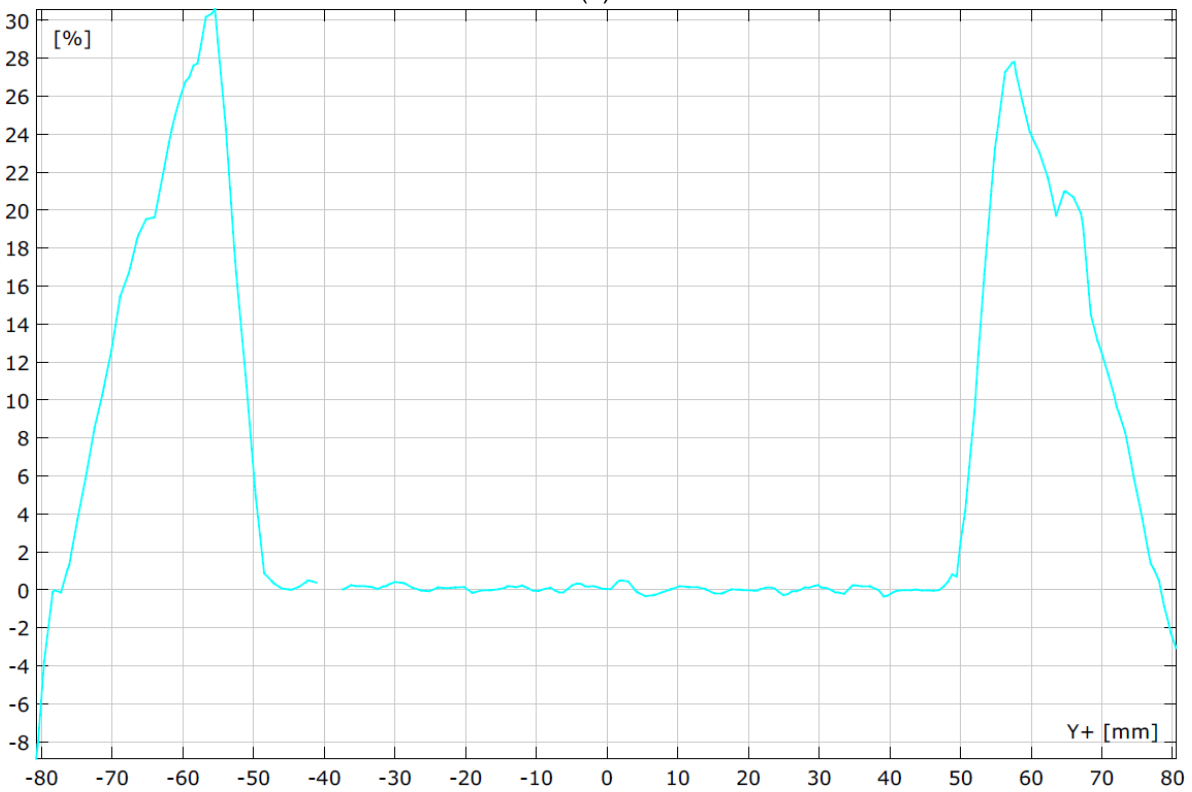


(b)

Fig.9: |Z-displacements| measured on the lower surface of the specimen at 98 s: (a) map, and (b) values along the intersection with the YZ-plane.



(a)



(b)

Fig.10: Thinning percentage on the lower surface of the specimen at 98 s: (a) map, and (b) values along the intersection with the YZ-plane.

Note: thinning is denoted by $-\varepsilon_3$ in GOM Correlate software. This quantity is not measured directly, but rather derived from major and minor strains using the principle of conservation of volume. If volume is assumed constant, then the product of all stretch ratios in the three principal directions is equal to one [13], such that

$$(1 + \varepsilon_1) (1 + \varepsilon_2) (1 - (-\varepsilon_3)) = 1$$

5 Simulations

Two different approaches were taken to model the SPIF process. The first approach was the traditional FEA approach, where all the parts were modelled using traditional shell finite elements. The second approach was a hybrid approach, where the blank was modelled using isogeometric shell elements and the remaining components (tool and upper and lower binders) were modelled using traditional shell finite elements. LS-DYNA enables the combination of FEA and IGA in a hybrid approach and in this case, the FEA blank was simply replaced by an IGA blank without further modifications. Upper and lower binders were in fact modelled with shells to achieve better accuracy. Constraining the clamped domain of the blank (outside the circular area) was another option, which was not pursued due to the required penalty-based boundary conditions for IGA.

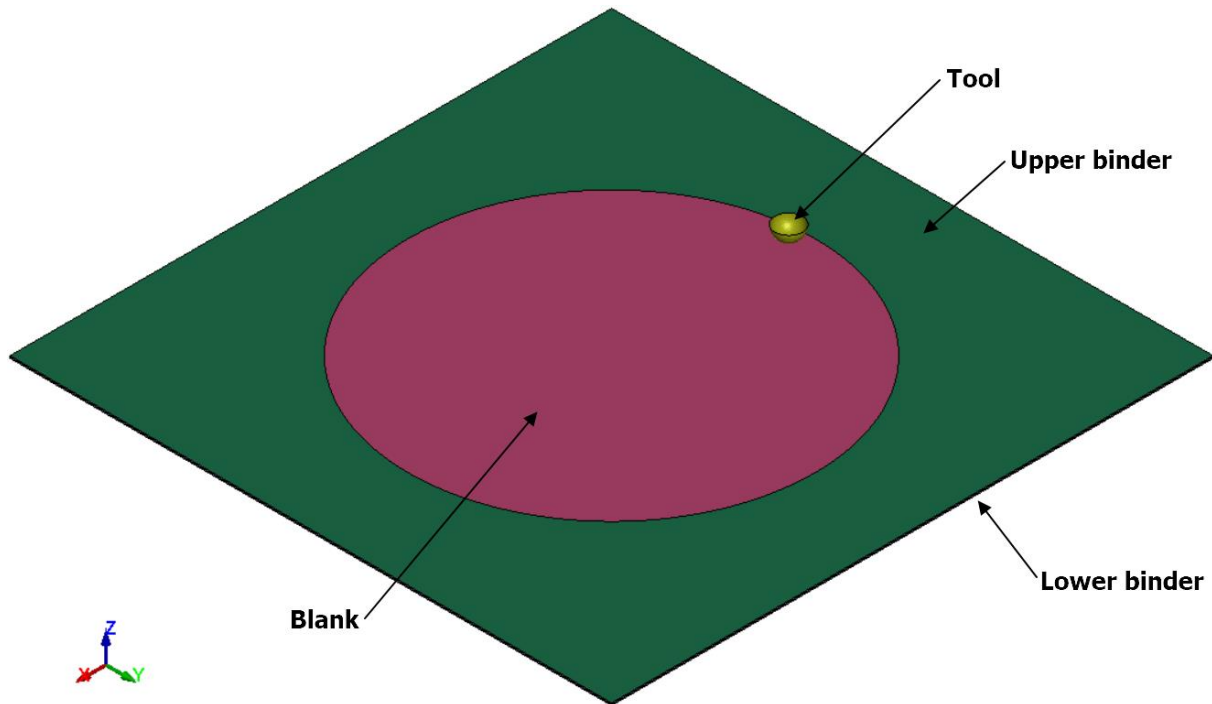


Fig. 11: Details of simulation models (mesh hidden).

Both the FEA and hybrid models were setup using LS-PrePost. However, the isogeometric blanks were setup using the IGA patch creation function with the “extend” option in ANSA, which extends the patch beyond the physical boundaries of the blank and then trims off the elements with smaller stable time steps at the patch boundary (open knot vector NURBS patch). Together with a suitable time step estimate in LS-DYNA (IGADO=1, see Section 5.2.1), this type of IGA patch enables a larger stable time step size of the blank. The units used were kg, mm, ms, kN, and GPa. An MPP development version of LS-Dyna with the latest IGA implementations available was used to solve all analyses on Australia’s Gadi high performance computer (HPC), with four CPUs assigned per analysis. The explicit time integration scheme was chosen after a review of the literature [14, 15]. Details of each analysis are tabulated in Table 1.

Model number	Analysis approach	Element edge length (mm) of the blank	Number of interpolation elements (NISR=NISS)	DT2MS	Percentage mass added
1.1	FEA	4	N/A	-0.001	74.236
1.2	FEA	2	N/A	-0.001	559.23
1.3	FEA	1	N/A	-0.001	2499.2
2.1	Hybrid	8	2	-0.001	0
2.2	Hybrid	6	2	-0.001	0
2.3	Hybrid	4	2	-0.0013	84.652
2.4	Hybrid	4	1	-0.0013	84.652
2.5	Hybrid	2	1	-0.0014	604.64
2.6	Hybrid	1	1	-0.00138	2518.8

Table 1: Description of analyses.

Different element edge lengths for the blank were used as a convergence study and to check whether, for a comparable simulation time, more accurate results are achieved with IGA. The element size for the tool and binders was kept constant at approximately 0.5 mm for all models. This meant that only the blank required editing between analyses, and that the tool and binders always provided a smooth contact surface. The NISR and NISS parameters, DT2MS parameters (minimum time step size), and percentage mass added columns are discussed in the sections that follow.

5.1 FEA

5.1.1 Model setup

The assumptions made during model setup were:

1. Negligible / no slippage occurred between the binders and blank.
2. The binders and tool are perfectly rigid.

Point 1 above allowed the use of keyword ***CONTACT_TIED_SHELL_EDGE_TO_SURFACE_BEAM_OFFSET** to tie the binders to the blank. Keyword ***CONTACT_AUTOMATIC_SURFACE_TO_SURFACE** was used to define touching contact between the blank and tool. Static and dynamic friction coefficients of 0.1 and 0.05, respectively, were assumed. Correctly characterising the friction coefficients is a subject for future work. For all contacts, the blank was defined as the SURFA (tracked) surface.

Regarding point 2 above, the binders and tool were assigned rigid material properties through the use of keyword ***MAT_RIGID**, where typical steel properties were assigned for contact purposes. The binders were fixed in space and the tool's rotations were constrained, except for rotation about its own axis. The keyword ***MAT_BARLAT_YLD2000** was used to define the material properties for the deformable blank. The properties were provided by ThyssenKrupp Rasselstein GmbH.

For computational efficiency purposes:

1. Mass scaling was applied to increase the time step and thus reduce solving time. The DT2MS parameter (refer to Table 1) was set the same for all FEA models; therefore, as the element size decreases, the amount of mass scaling increases. However, the DT2MS parameter (and thus the time step) was increased for each IGA analysis to provide a similar amount of added mass when

compared to its equivalent FEA counterpart (i.e., FEA and hybrid models having the same element edge length).

2. An artificially high tool velocity was assigned to reduce solving time. According to reference [15], a maximum tool velocity of 2 mm/ms is recommended. The average tool velocity assigned in this paper's analyses was 1.7875 mm/ms through the use of prescribed X-, Y-, and Z-displacements (keyword ***BOUNDARY_PRESCRIBED_MOTION_RIGID** with VAD equal to 2).
3. The number of integration points through the element thickness (NIP) was set to 3 to reduce solving time.

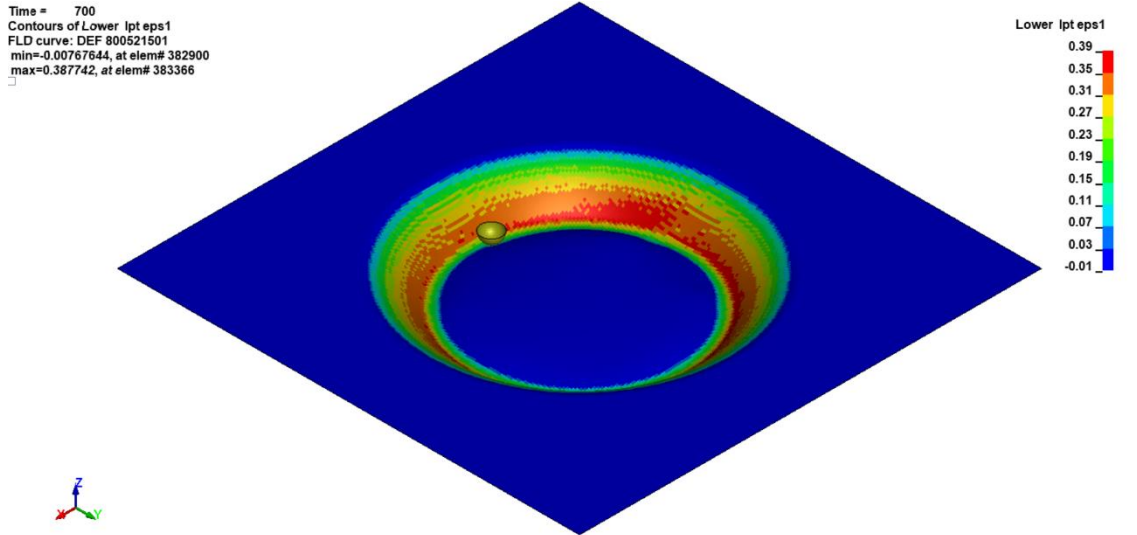
The first two points above may have an effect on the inertia of the blank; however, a detailed study of their influence has not been investigated (note that significant amounts of mass scaling were reported as shown in Table 1; however, the global energies seemed okay). The deformation of the blank is assumed to be quasi-static due to the time taken for the physical process to occur; therefore, critical damping was applied to the analyses using keyword ***DAMPING_GLOBAL**. An eigenvalue analysis was performed to calculate the critical damping constant.

The blank was meshed using four-noded shell elements with C^0 inter-element continuity and linear basis functions. In keyword ***SECTION_SHELL**, ELFORM was set to 16 (fully integrated Reissner-Mindlin shell element with 2x2 integration points in the shell plane).

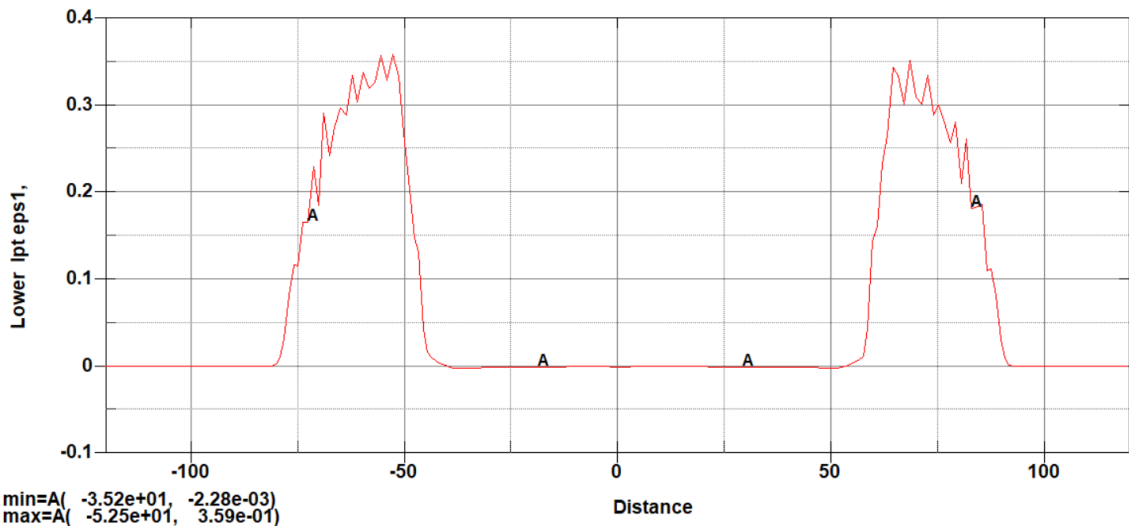
5.1.2 Results

Since the velocity of the tool was scaled in the simulation models, the simulation times and experimental times are non-coincidental. The simulation time used for the results is 700 ms, whereas the termination time for the analyses was 1600 ms. When comparing run / solve times between analyses, 1600 ms is used. Since the tool velocity was constant in the simulations and variable in the experiment, corresponding times were determined based on tool rotation angle. The relationship between tool rotations and forming depth for the simulation and experiment correlated well until 700 ms (98 s in the experiment), after which the correlation deteriorated slightly. The relationship between tool rotations and forming depth for the experiment became nonlinear after 98 s which contradicted the programming of the toolpath. This finding brought the accuracy of the DIC measurement beyond 98 s into question and the decision was taken to compare the simulations at this point. Only the elasto-plastic regime is considered in this study as failure / damage data was unavailable for simulation purposes.

Fringe plots of the maximum principal strains, Z-displacement, and thinning are shown below for model 1.3. Isometric views from above are used for the fringe plots, and the results shown correspond to the lower surface of the blank due to the experimental setup (i.e., the DIC system was placed underneath the blank). It is also where the most strain is seen in the simulations.



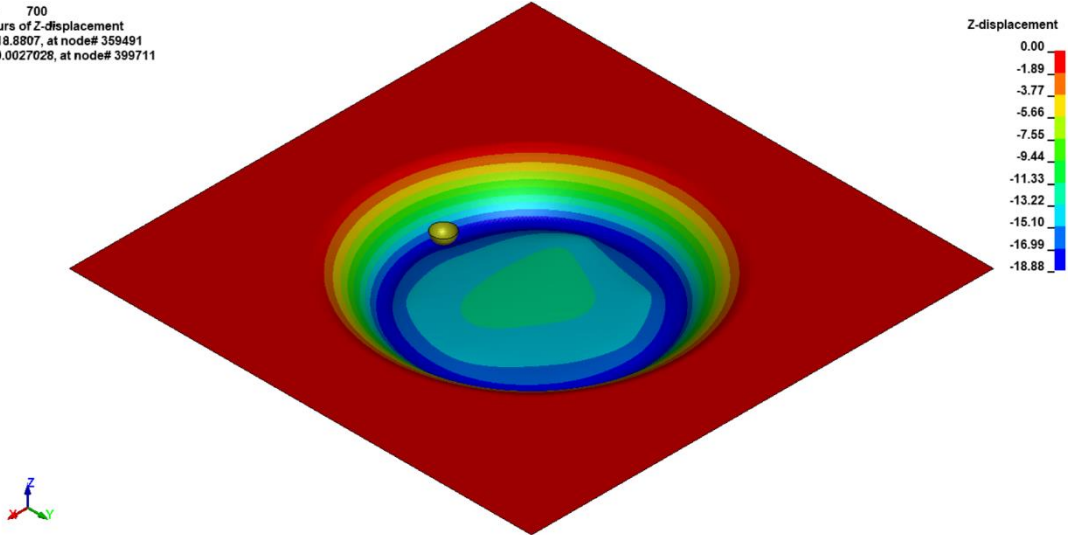
(a)



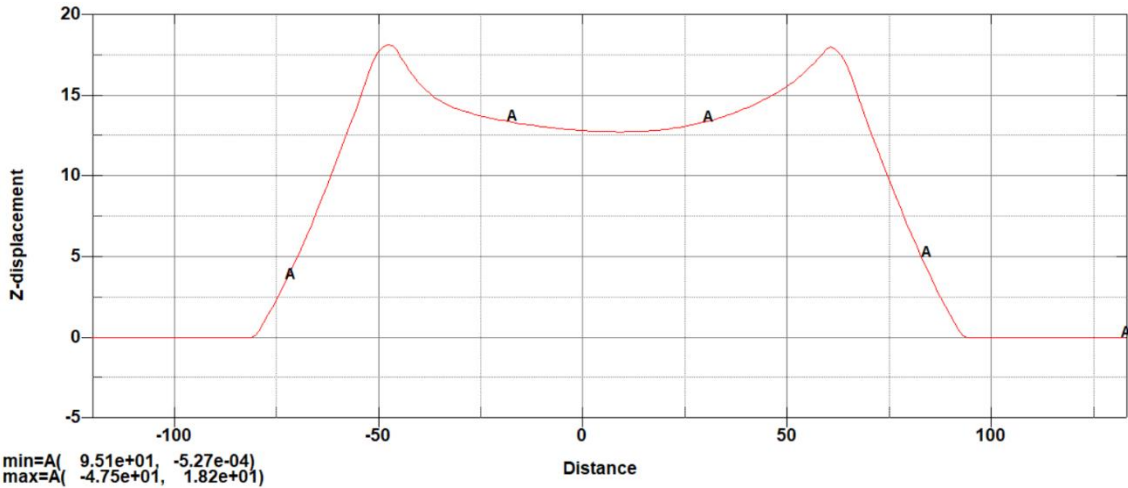
(b)

Fig.12: FEA model 1.3: Maximum principal strain at 700 ms: (a) fringe plot and (b) results on the YZ plane.

Time = 700
Contours of Z-displacement
min=-18.8807, at node# 359491
max=0.0027028, at node# 399711



(a)



(b)

Fig.13: FEA model 1.3: Maximum |Z-displacement| (mm) at 700 ms: (a) fringe plot and (b) results on the YZ plane.

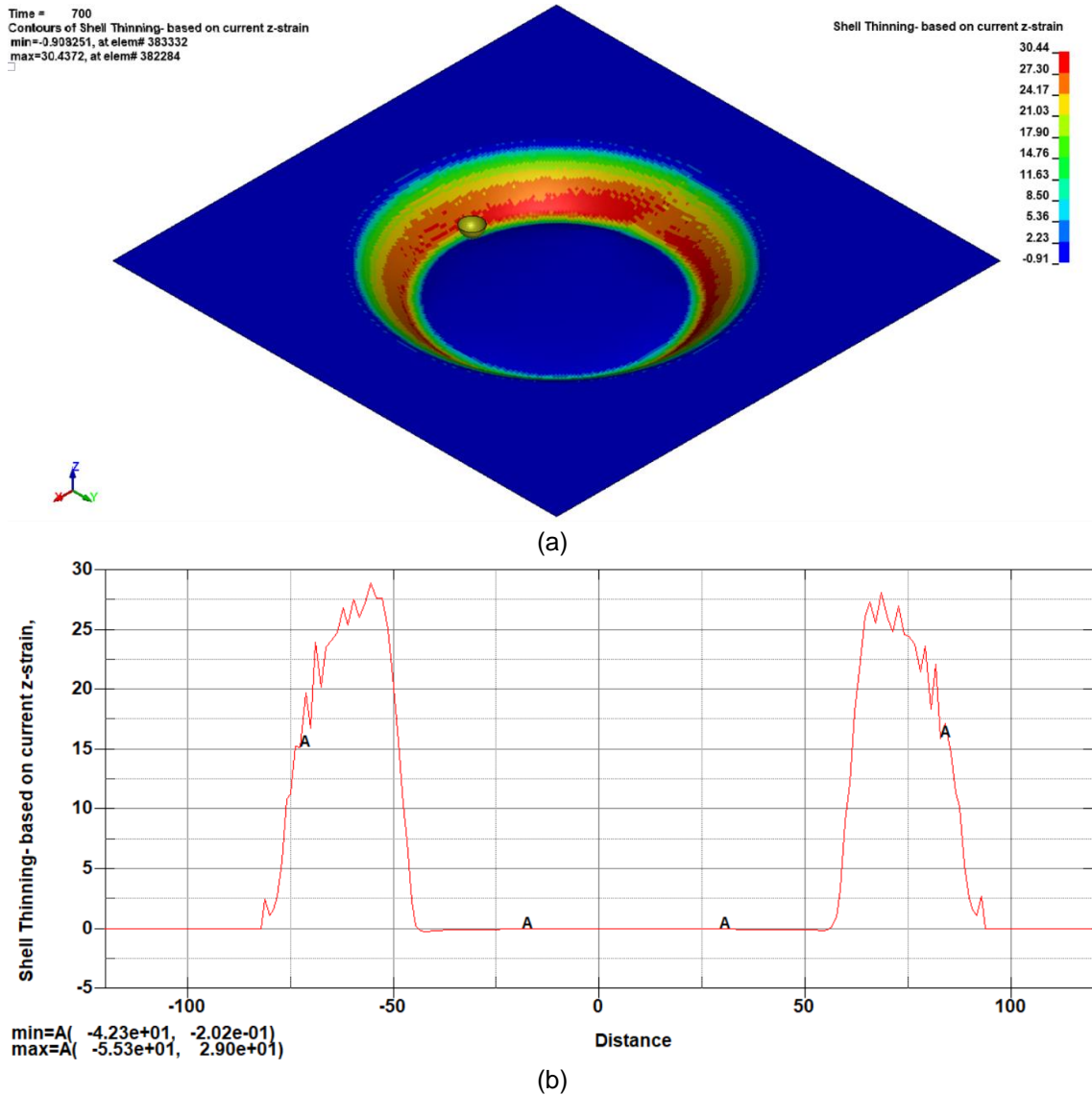


Fig. 14: FEA model 1.3: Thinning (%) at 700 ms: (a) fringe plot and (b) results on the YZ plane.

5.2 IGA

5.2.1 Model setup

The setup for the hybrid model was similar to the FEA model except for a few small changes detailed in this section; notably, the blank was changed to an IGA part using C^1 – quadratic isogeometric shell elements. For keyword `*SECTION_IGA_SHELL`, `ELFORM` was set to 3 (Reissner-Mindlin shell) and `IRL` set to 0 (reduced Gauss-Legendre quadrature leading to 2x2 integration points per element).

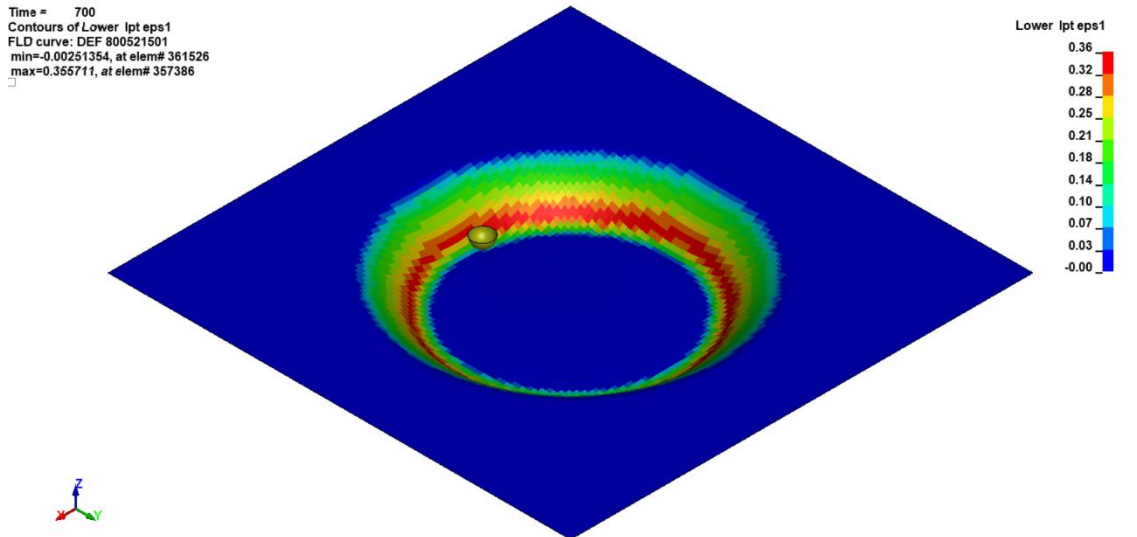
In keyword `*CONTROL_TIMESTEP`, `IGADO` was set to 1 to take advantage of a larger stable time step for the isogeometric elements of the blank, enabled by the ANSA “extend” option during IGA patch creation as mentioned above. With these settings, the stable time step of quadratic IGA elements is around 25% higher compared to conventional linear finite elements [7] (for the same element size). As described in Section 5.1.1, a larger time step (for a similar amount of mass scaling) was used for the models with the IGA blank to speed up the simulations. Alternatively, a constant predefined time step together with mass scaling could have been used for all models, which would result in less artificial mass being added for the IGA blank.

Contact treatment between the tool and blank was done via an interpolation mesh by setting `IGACTC` equal to 0 in `*CONTROL_CONTACT`. Therefore, the same contact definitions for tied and surface to surface contacts (as for FEA) could be used without modifications. The number of interpolation elements per isogeometric element was defined using `NISR` and `NISS` in keyword `*IGA_SHELL` (refer to Table

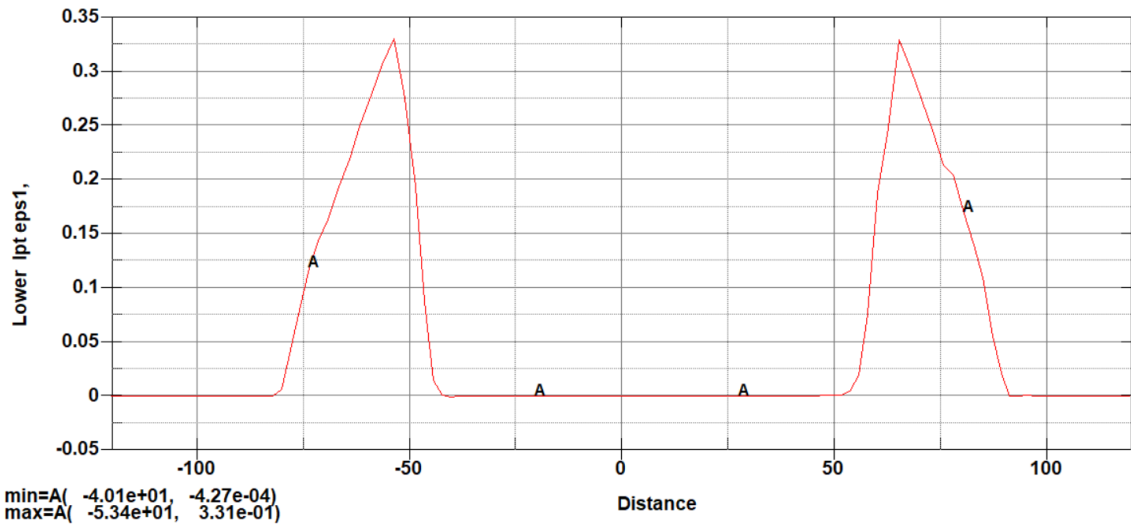
1). This is a benefit of IGA / hybrid analyses, where the “mechanical” mesh and the “contact” mesh may be decoupled. The interpolation elements do not affect the time step. Models 2.3 and 2.4 are identical, except for the NISR and NISS values. This was done to check their effect, if any, on the analyses.

5.2.2 Results

The results presented here match the same format as used for the FEA results section.



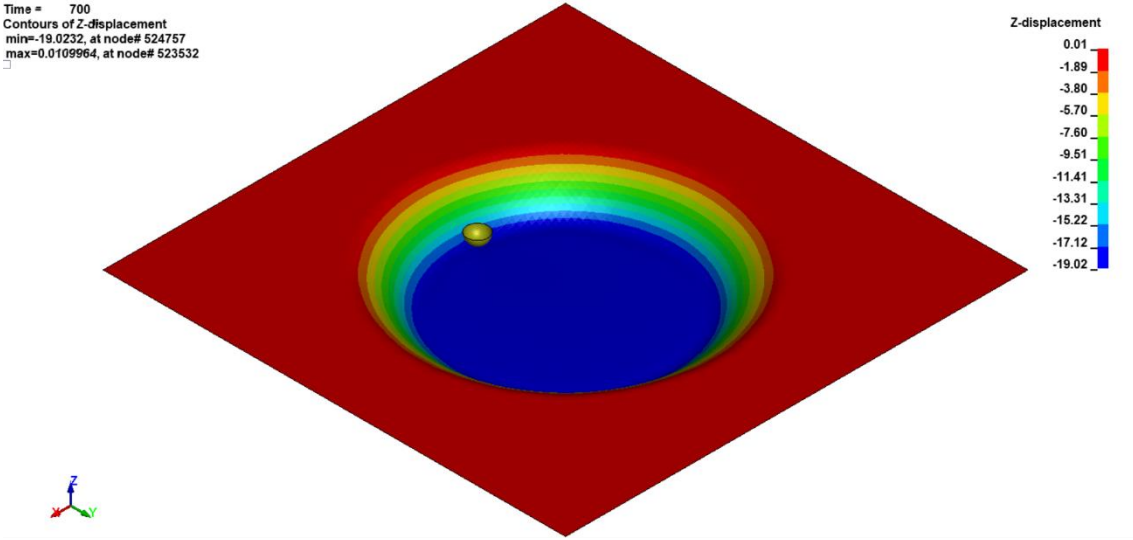
(a)



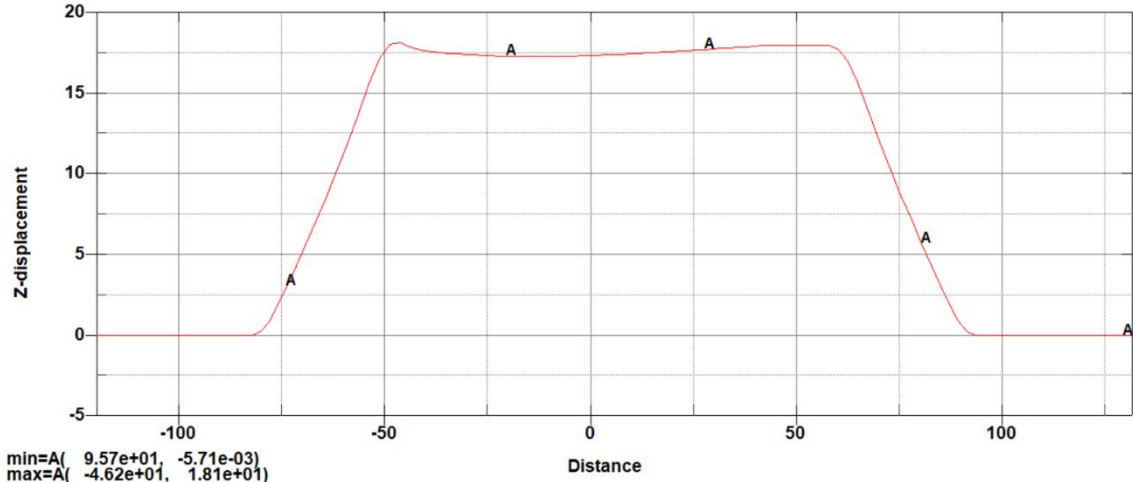
(b)

Fig. 15: Hybrid model 2.5: Maximum principal strain at 700 ms: (a) fringe plot and (b) results on the YZ plane.

Time = 700
Contours of Z-displacement
min=-19.0232, at node# 524757
max=0.0109964, at node# 523532



(a)



(b)

Fig. 16: Hybrid model 2.5: Maximum |Z-displacement| (mm) at 700 ms: (a) fringe plot and (b) results on the YZ plane.

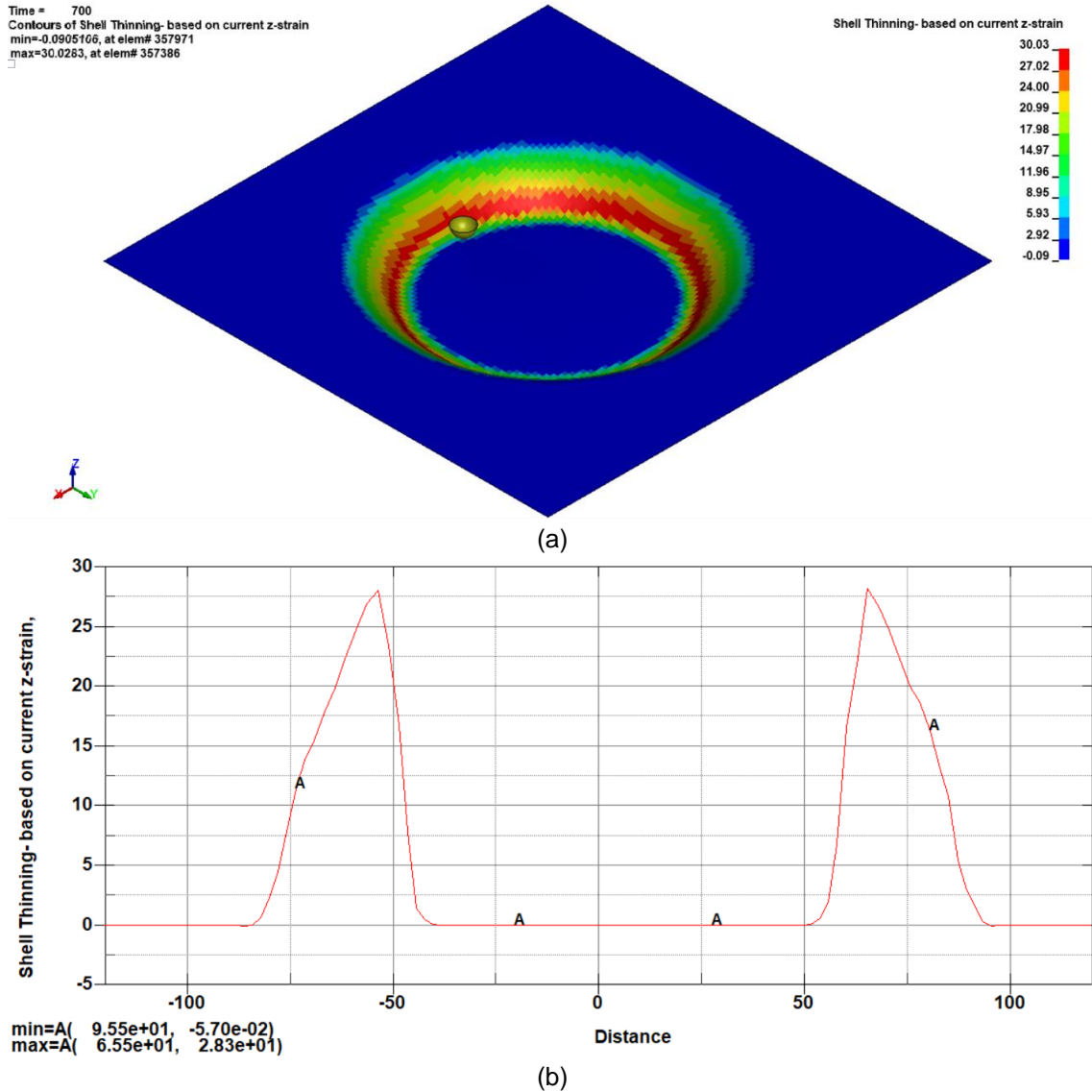


Fig. 17: Hybrid model 2.5: Thinning (%) at 700 ms: (a) fringe plot and (b) results on the YZ plane.

6 Discussion

The SPIF model in this paper is not a good case study for evaluating the modelling effort between FEA and IGA due to the simplicity of the geometry (i.e., the reduction in meshing effort was negated for IGA). The modelling effort was therefore the same for FEA as it was for IGA in this paper.

The results along the YZ plane for all simulation models are plotted and overlaid with the experimental results in the images that follow.

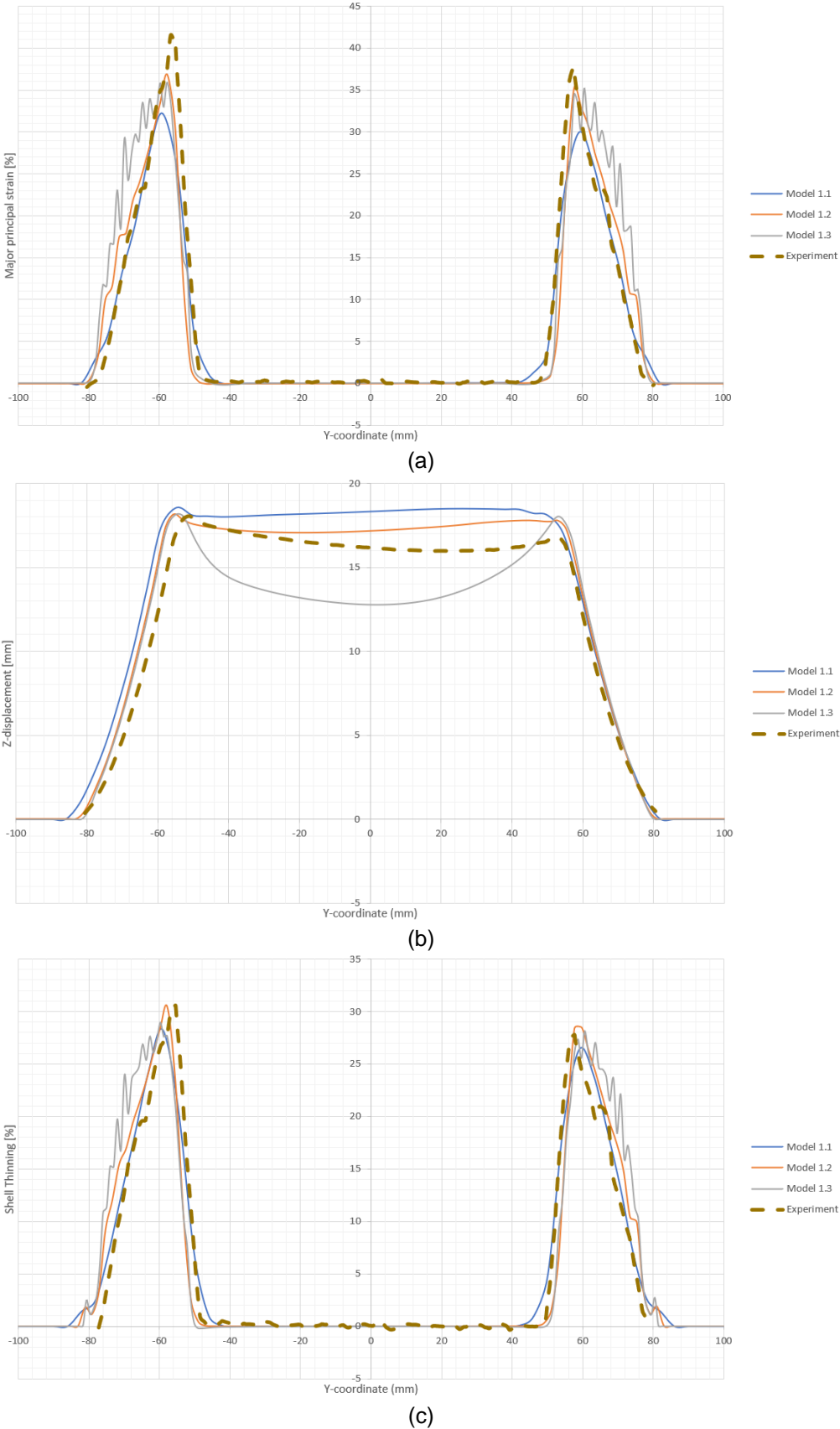
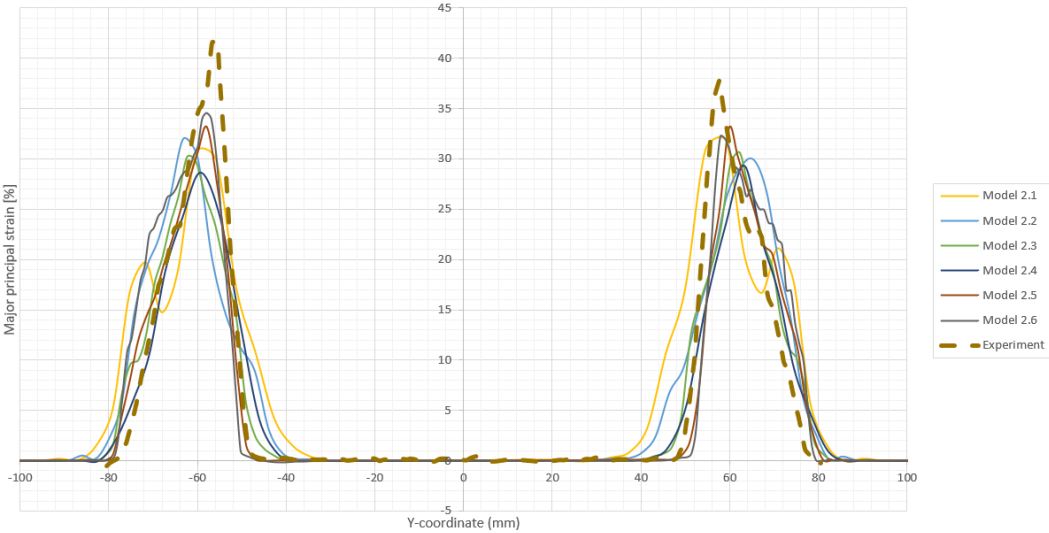
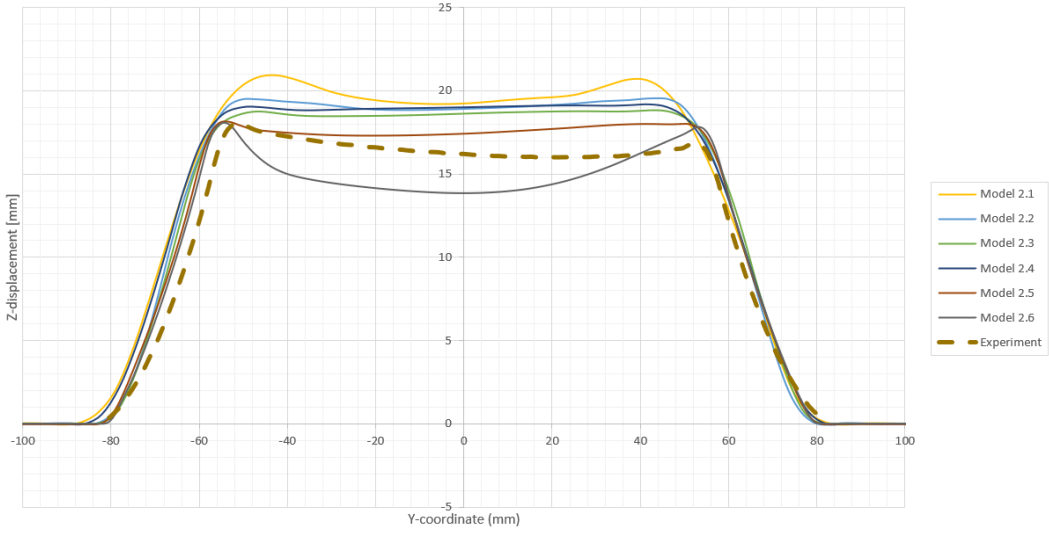


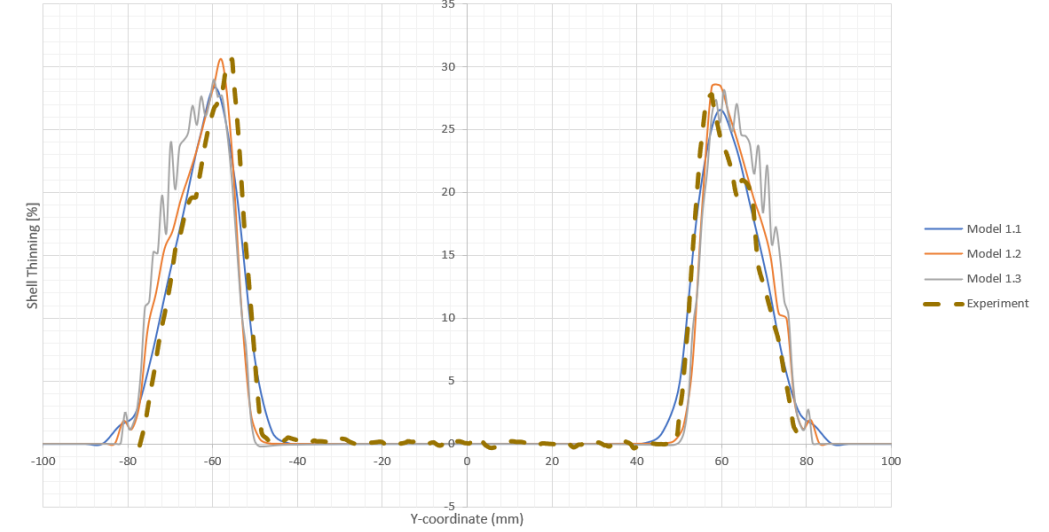
Fig. 18: FEA results along the intersection with the YZ-plane at 700 ms: (a) major principal strain (%), (b) |Z-displacement| (mm) and (c) thinning (%).



(a)



(b)



(c)

Fig. 19: IGA results along the intersection with the YZ-plane at 700 ms: (a) major principal strain (%), (b) |Z-displacement| (mm) and (c) thinning (%).

The Z-displacements indicate that the strain and thinning results could be compromised, as highlighted in Figure 20. The main concern is the large concave “bulge” seen in the centre portion of the graph, which corresponds to the model with the finest mesh. It is believed this could be a result of significant time scaling and mass scaling, which affect the inertia of the blank; however, this requires further investigation. Another observation from Figure 20 is that the models with large element sizes fail to capture bend radius accurately. It was confirmed that the tool was tracking along the correct path.

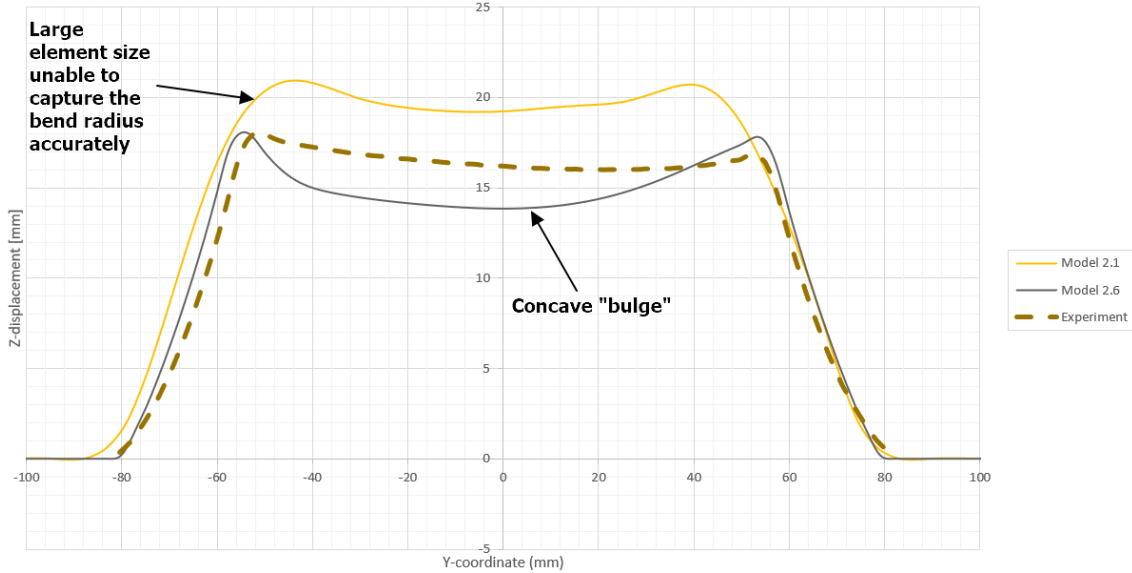


Fig.20: $|Z\text{-displacement}|$ (mm) results at 700 ms on the YZ plane for hybrid models 2.1 and 2.6, overlaid with the experimental result.

Importantly, more than a single set of experimental data is required to make definitive conclusions about the accuracy of IGA versus FEA (repeatability and scatter are unknown). Additionally, better alignment of timescales is required for future work. Despite the previously mentioned concerns, from a qualitative point of view, the results do seem plausible.

For convenience, the maximum experimental results are tabulated below.

	Max. principal strain (%)	Max. Z-displ. (mm)	Max. thinning (%)
Experimental value	41.6	18.1	30.6

Table 2: Experimental results at 98 s (simulation time of approximately 700 ms).

A summary of the simulation results is provided in Table 3, along with the solution runtimes (to reach 1600 ms). The values are acquired from the graphs shown previously.

Model number	Max. prin. strain (%)		Max. Z-displ. (mm)		Max. thinning (%)		Runtime (hh:mm:ss)
	Sim.	Deviation (%)	Sim.	Deviation (%)	Sim.	Deviation (%)	
1.1	32.2	22.6	18.5	2.2	28.3	7.5	05:01:17
1.2	36.8	11.5	18.2	0.6	30.4	0.7	10:56:33
1.3	35.9	13.7	18.2	0.6	29.0	5.2	30:28:09
2.1	31.9	23.3	20.9	15.5	26.8	12.4	02:51:18
2.2	32.0	23.1	19.5	7.7	28.6	6.5	04:09:10
2.3	30.6	26.4	18.8	3.9	27.1	11.4	05:50:42
2.4	29.3	29.6	19.2	6.1	26.2	14.4	04:55:59
2.5	33.1	20.4	18.1	0.0	28.3	7.5	11:38:57
2.6	34.5	17.1	18.1	0.0	28.7	6.2	31:22:28

Table 3: Summary of results at 700 ms and the solution times to reach 1600 ms. The “deviation” columns refer to the difference between the simulation and experimental results.

IGA has a greater computational cost per element compared to traditional FEA; however, a larger time step may be used for a similar amount of mass scaling. Using this approach, comparable runtimes are observed between IGA and FEA. The future hope is to use larger element sizes for IGA due to its higher accuracy (i.e., higher continuity and element order) compared to FEA, which will further reduce IGA runtimes. Comparing models 2.3 and 2.4, increasing the number of interpolation elements also increases analysis runtime, and accuracy is affected. This was expected due to a change in contact resolution.

7 Literature

- [1] Zhu, G., et al., 2022. *Roadmap to Advance Heliostat Technologies for Concentrating Solar-Thermal Power* (No. NREL/TP-5700-83041). National Renewable Energy Lab.(NREL), Golden, CO (United States).
- [2] U.S. Department of Energy. (2022) Crescent Dunes Solar Energy Project. Available at: <https://solarpaces.nrel.gov/project/crescent-dunes-solar-energy-project> (Accessed: 13 October 2023).
- [3] Malhotra, R., Xue, L., Belytschko, T. and Cao, J., 2012. Mechanics of fracture in single point incremental forming. *Journal of Materials Processing Technology*, 212(7), pp.1573-1590.
- [4] Jackson, K. and Allwood, J., 2009. The mechanics of incremental sheet forming. *Journal of materials processing technology*, 209(3), pp.1158-1174.
- [5] Hughes, T.J.R., Cottrell, J.A., Bazilevs, Y.: "Isogeometric Analysis: CAD, finite elements, NURBS, exact geometry, and mesh refinement", *Computer Methods in Applied Mechanics and Engineering*, Vol. 194, 2005, 4135-4195.
- [6] J.A. Cottrell, T.J.R. Hughes, A. Reali, Studies of refinement and continuity in isogeometric structural analysis, *Comput. Methods Appl. Mech. Eng.* 196 (2007) 4160–4183.
- [7] Leidinger, L., "Explicit Isogeometric B-Rep Analysis for Nonlinear Dynamic Crash Simulations", PhD Thesis, Technical University of Munich, Germany, 2020.
- [8] Leidinger, L., Hartmann, S., Benson, D., Nagy, A., Rorris, L., Chalkidis, I., Bauer, F.: "Hybrid IGA/FEA Vehicle Crash Simulations with Trimmed NURBS-based Shells in LS-DYNA", 13th European LS-DYNA Conference 2021, Ulm, Germany.
- [9] Hartmann, S., Benson, D., Li, L., Nagy, A.: "Sheet Metal Forming Simulation with IGA in LS-DYNA", 15th International LS-DYNA Users Conference 2018, Detroit, US.
- [10] Hollweck, C., Leidinger, L., Hartmann, S., Li, L., Wagner, M., Wüchner, R.: "Systematic assessment of isogeometric sheet metal forming simulations based on trimmed, multi-patch NURBS models in LS-DYNA", 14th European LS-DYNA Conference 2023, Baden-Baden, Germany.
- [11] Meßmer, M., Leidinger, L., Hartmann, S., Bauer, F., Duddeck, F., Wüchner, R., Bletzinger, K.-U.: "Isogeometric Analysis on Trimmed Solids: A B-Spline-Based Approach focusing on Explicit Dynamics", 13th European LS-DYNA Conference 2021, Ulm, Germany.
- [12] Holmes, J., Sommacal, S., Das, R., Stachurski, Z. and Compston, P., 2023. Digital image and volume correlation for deformation and damage characterisation of fibre-reinforced composites: A review. *Composite Structures*, p.116994.
- [13] Carl Zeiss GOM Metrology GmbH. (2022) GOM Software 2022. In: Zeiss Quality Tech Guide. Available at: https://techguide.zeiss.com/en/gom-software-2022/article/cmd_comparison_check_scalar_thickness_reduction.html (Accessed: 13 October 2023).
- [14] Ren, F., Cui, Z., Xia, Z.C., Slavik, T., Zhang, L. and Zhu, X., 2010. Process Modeling of Freeform Incremental Forming Using LS-DYNA. In *11th International LS-DYNA Users Conference of Metal Forming*.
- [15] Maker, B.N. and Zhu, X., 2000. Input parameters for metal forming simulation using LS-DYNA. *Livermore Software Technology Corporation*, 4, pp.43-46.